ELSEVIER

Journal of Fluids and Structures 19 (2004) 1005–1025

JOURNAL OF FLUIDS AND STRUCTURES

www.elsevier.nl/locate/jnlabr/yjfls

Effect of opening obstructions on the flow-excited response of a Helmholtz resonator

P.J. Zoccola Jr.*

Naval Surface Warfare Center, Carderock Division, Code 725, 9500 MacArthur Boulevard, West Bethesda, MD 20817-5700, USA

Received 15 January 2003; accepted 22 April 2004

Available online 22 July 2004

Abstract

Flow over cavity-backed openings often results in high-amplitude pressure fluctuations inside the cavity. This phenomenon is known to be caused by periodic vortex shedding from the upstream edge of the opening becoming coupled to a resonance frequency of the cavity. These fluctuations are frequently suppressed in practice by installing a grid in the opening. Analysis of results from large-scale model tests has revealed that even with a grid present, under some circumstances these fluctuations continue to occur, at amplitudes and frequencies similar to those that would be observed for an unobstructed opening. This study is an experimental effort to understand why and under what circumstances this flow-excited resonance continues to occur despite the presence of a grid. Measurements of cavity pressure due to flow over a cavity with obstructions or grids of varying dimensions in the opening were made. Measurements were also made of the flow field in the cavity opening for selected configurations. It was seen that the frequency of the excitation and the amplitude of the response at the large length scale are altered in various ways, depending on the configuration of the grid. Of particular interest is the distinct difference between the results obtained with coarse and fine grids. Flow field results show the effects that a grid has on the flow, including effects on the vortex convection velocity and the energy production distribution.
Published by Elsevier Ltd.

Keywords: Cavity resonance; Sheartone; Vortex convection; Flow excitation

1. Introduction

Fluid flow over a surface with a cavity-backed aperture may, under certain conditions, result in pressure fluctuations within the cavity, which can be quite high in amplitude. The presence of these fluctuations, referred to as a flow-induced cavity resonance, is frequently a problem in aircraft, marine vessels, and other applications.

A flow-induced cavity resonance results from the interaction of the fluctuations in the shear layer over the opening with the resonant response of the cavity. The shear layer that forms over the cavity opening is unstable and rolls up into discrete vortices. The presence of the downstream edge causes these structures to become highly organized at a discrete frequency (Rockwell and Knisely 1979). The frequency of the organized flow is proportional to the free-stream velocity, U_0, of the flow and inversely proportional to the length, L, of the opening, resulting in a constant Strouhal number, $\mathrm{St} = fL/U_0$, for a given configuration. This phenomenon may be observed in measurements of fluctuating pressure beneath the aperture and these speed-dependent tones are referred to as sheartones. The terms "first sheartone" and "second sheartone" are used to refer to the presence of one and two vortices, respectively, in the cavity opening. When

*Tel.: +1-3012272403; fax: +1-3012274405.
E-mail address: zoccolapj@nswccd.navy.mil (P.J. Zoccola Jr.).

0889-9746/$ - see front matter Published by Elsevier Ltd.
doi:10.1016/j.jfluidstructs.2004.04.013

Nomenclature

f	frequency
f_h	Helmholtz frequency of cavity
H	shape factor
k	wave number
l	length of obstruction element in streamwise direction
L	length of cavity opening in streamwise direction
q	dynamic head, $\frac{1}{2}\rho U_0^2$
St	Strouhal number, fL/U_0
U_0	free-stream velocity
U_c	convection velocity
$\mathbf{u}$	velocity vector
u^*	shear velocity
v'	fluctuating component of velocity in the y direction
v^*	nondimensional velocity, U_0/fL
W_v	power extracted from mean flow
δ	boundary layer thickness
δ^*	displacement thickness
θ	momentum thickness
ρ	density
ϕ	phase
$\boldsymbol{\Omega}$	vorticity vector
Ω_3'	fluctuating vorticity in z direction

the sheartone frequency approaches a resonance frequency of the cavity, which may be the Helmholtz resonance or an acoustic standing wave, the vortex formation process and the cavity resonant response become coupled, forming a flow-induced cavity resonance. The terms flow-induced cavity resonance or resonant sheartone are used to describe the tone measured in the cavity pressure spectrum at speeds where the vortex shedding is coupled with the cavity response; nonresonant sheartone describes these tones where coupling is not present. A flow-induced cavity resonance results in high-amplitude pressure fluctuations in the cavity. It also alters the dependence of frequency on U_0 and, hence, alters St.

Elder (1978) and Mast and Pierce (1995) showed how the frequency of flow-induced cavity resonance could be predicted by using a root-locus technique to extract eigenvalues from the controlling feedback relationships. A similar approach was taken by Kook and Mongeau (2002), who were able to also predict the amplitude of the cavity pressure fluctuations. This technique is only applicable at conditions where coupling between the vortex shedding and the cavity resonance exists. It is often desirable to predict the frequencies of nonresonant sheartones. Howe (1997) describes an analytical technique for determining the Strouhal number of the shear layer disturbance in the absence of a resonance. However, his results are applicable only for very thin shear layers, DeMetz and Farabee (1977) performed extensive measurements of fluctuations from flow over a cavity-backed aperture over a broad speed range. Their results show that the Strouhal number of sheartones depends on the ratio δ/L, where δ is the boundary layer thickness. In their experiment, the ratio was changed by varying L, while δ remained constant.

The presence of unwanted flow-induced cavity fluctuations is frequently remedied by the installation in the opening of a grid of some sort, such as louvers or a perforated plate. Though it can produce unwanted broadband noise (Looijmans and Bruggeman 1997; Nelson 1982) and can also result in tones due to vortices shed over individual holes (Tsui and Flandro 1977), this has been an effective way to eliminate the tone due to excitation at the overall opening length scale, L. However, analysis of results from unpublished large-scale model tests where a perforated plate was installed over a cavity-backed opening showed tones occurring at amplitudes and frequencies similar to what would be observed for an uncovered opening. In addition, Celik and Rockwell (2002) reported shear layer oscillation with a perforated plate that was similar to that which would be observed with no plate present. Their measurements were made with no resonator present. These results warrant further exploration of flow-induced oscillations in the presence of a grid.

The approach taken in this study was to first consider the effect of a single obstruction in the opening and examine its effects on the cavity pressure fluctuations and the flow field. Obstructions of various sizes and in openings of various sizes were considered. In addition, grids with varying numbers of elements were considered. The flow-excited cavity

problem is commonly treated as a two-dimensional flow [Rockwell and Naudascher (1978)]. Accordingly, in this experiment, the grids studied were two dimensional, consisting of a series of linear elements in the plane of the opening and aligned normal to the direction of fluid flow.

2. Experimental arrangement

The experiment was conducted in the Anechoic Flow Facility (AFF) at the Naval Surface Warfare Center, Carderock Division (NSWCCD). The AFF is a low-noise closed-loop wind tunnel with a 2.4 m high × 2.4 m wide × 5.8 m long closed jet test section leading into a 6.3 m long × 6.9 m wide × 6.9 m open jet test-section surrounded by an anechoic room. A more detailed description of this facility may be found in Farabee and Casarella (1984).

A 2.4 m long × 1.8 m high plate was mounted so that it constituted an extension into the anechoic section of the closed jet section wall. Therefore, the boundary layer over the plate was a continuation of the fully developed equilibrium boundary layer on the test-section wall. A framed cut-out opening in the plate functioned as the cavity orifice. The frame allowed various opening configurations to be installed for testing. The cavity was a 0.53 m long × 0.73 m deep × 0.88 m high box, which was mounted behind the opening on the back of the plate, out of the flow stream. The depth of the cavity could be controlled by changing the position of a false bottom. A dimensional drawing of the plate and cavity fixture is shown in Fig. 1.

Measurements of the boundary layer 0.13 m upstream of the opening were made on the test plate as part of a prior experiment (Grega and Farabee 1997). A pitot tube was used to make measurements at a free-stream velocity of 32 m/s. The free-stream velocity in the wind tunnel was measured using pressure taps upstream and downstream of the contraction section of the wind tunnel. Fig. 2 is a plot of the boundary layer profile at that location. Boundary layer parameters were calculated and are shown in Table 1.

Fluctuating pressures inside of the cavity were measured using a 12.7 mm B&K microphone mounted on the top surface of the cavity interior, as indicated in Fig. 1. The signal from the microphone was amplified using an Ithaco amplifier and then digitized using a Hewlett Packard model 3566A Signal Processor. Power spectra were computed and

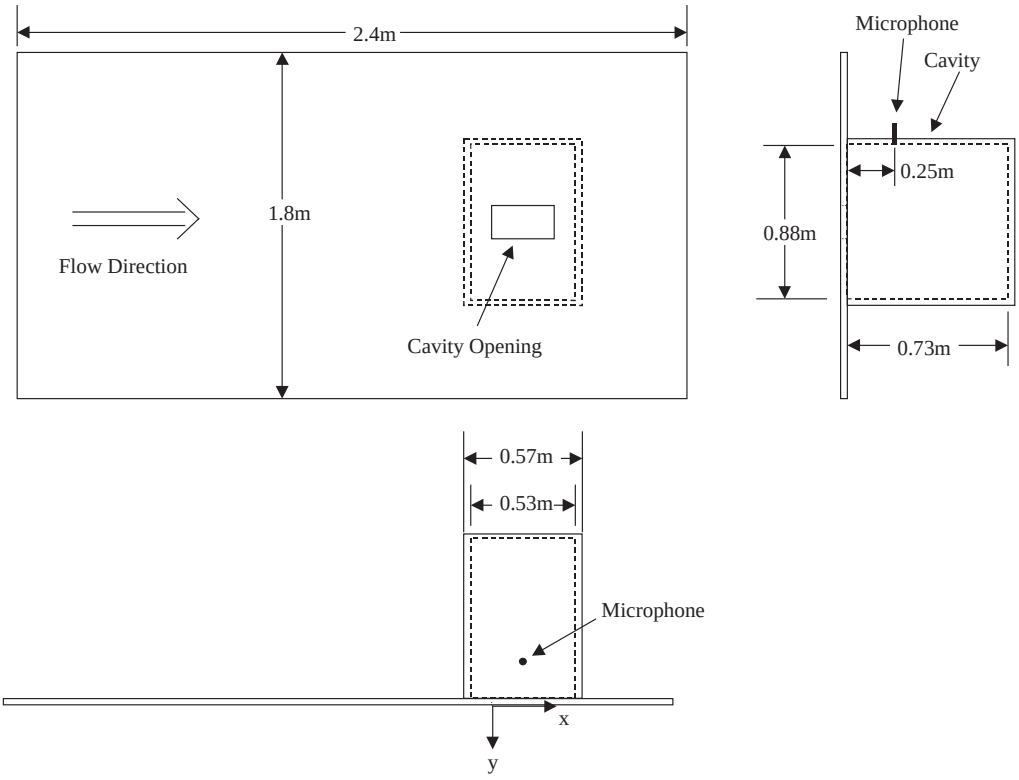

Fig. 1. Dimensional drawing of test plate and cavity showing flow direction and microphone location.

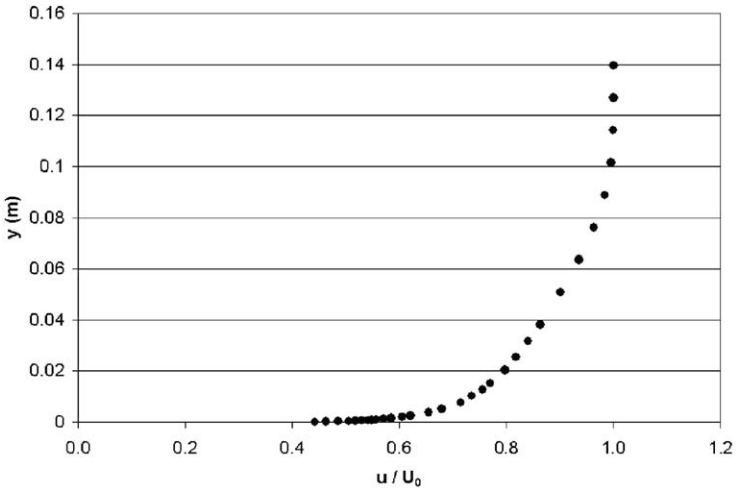

Fig. 2. Boundary layer profile made 0.13 m upstream of cavity opening at free-stream velocity of 32 m/s.

Table 1
Boundary layer properties 0.13 m upstream of cavity opening

U_0(m/s)	u^*(m/s)	δ (*m*)	δ^* (m)	θ (m)	$H=\delta^*/\theta$
32.2	1.09	0.096	0.0127	0.010	1.27

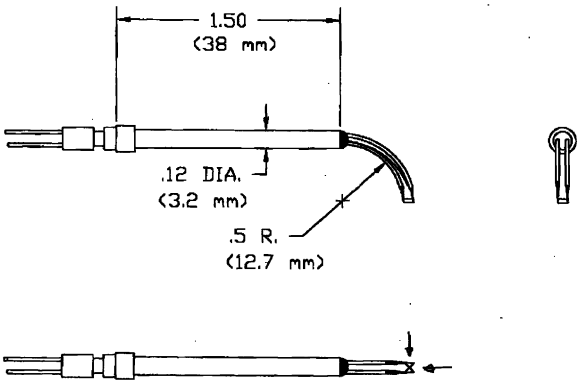

Fig. 3. Dimensional drawing of *x*-wire probe used to make constant temperature anemometer measurements of fluid velocity in the cavity opening.

stored on a personal computer. For all cavity pressure spectral measurements, 75 averages of a 1600 point fft over a frequency range of 0–400 Hz were used. All levels reported are at 1 Hz bandwidth.

Constant temperature anemometry (CTA) was used to measure the velocity field in the opening. A TSI IFA 300 anemometer was used with a custom designed *x*-wire probe. This probe was a commercially available TSI boundary layer probe, which was rewired so that sensing wires lie in the *x*–*y* plane while the prongs are in the *y*–*z* plane. This allowed the probe to be positioned close to the downstream edge of the opening. A drawing of this probe is given in Fig. 3. The probe was calibrated in the AFF. Measurements were made at 11 speeds and at five probe angles. Calibration coefficients were calculated using software supplied by TSI. This software indicated that the measurement error for fluid velocities is less than 5%.

A three axis traverse system was used for positioning the probe. The probe and the anemometer were controlled from a PC using LabView software. Data acquisition was also performed with LabView. The cavity pressure signal was

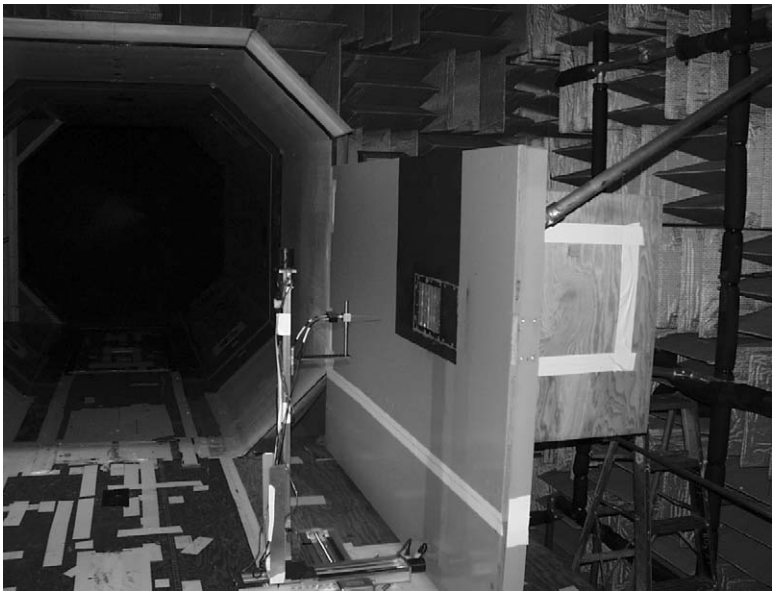

Fig. 4. Photograph of test plate and cavity installed in the wind tunnel. View is looking upstream from anechoic section into closed jet section. Traverse system and probe support are visible in front of the cavity opening.

acquired simultaneously with the velocity signals from the anemometer. Fig. 4 is a photograph showing the plate mounted in the anechoic section of the wind tunnel, with the traverse system and cavity visible.

The experiment was conducted in two phases. The first phase was intended to study the effect of a single obstruction in the opening. In the second phase, multiple obstructions were placed in the opening, dividing it into as many as 24 divisions. In both phases, cavity pressure was recorded over a range of tunnel free-stream velocities so that the amplitude and frequency of individual tones as a function of speed could be plotted. Flow field measurements of selected conditions were also made during both phases. Table 2 describes each of the tested configurations. Size of the opening, depth of the cavity, and size and depth of the obstructions are listed. In Fig. 5, drawings of some representative cavity opening configurations are shown. Included are several configurations with irregular spacing of obstructions. These were tested as part of the second phase of the experiment and are discussed in Section 3. The configuration with the largest number of obstructions (23) had the effect of covering 27% of the opening area. This would be expected to change the impedance of the opening and reduce the Helmholtz resonance frequency of the cavity. A lower resonance frequency for the cavity was seen; however, the difference in frequency was less than would be predicted, given the area reduction.

For all configurations, flow excited the cavity at its Helmholtz resonator mode. For the 190 mm deep cavity, the Helmholtz resonance frequency was 65 Hz; for the 690 mm depth, the frequency was 40 Hz. For all cases measured, the value of the depth, D, was greater then the boundary layer thickness and greater than the length of the opening. The effect of the ratios L/D and D/δ on the measured Strouhal number for rectangular cavities is discussed by Rockwell and Naudascher (1978) and Sarohia (1977), respectively. In general, the depth only influences St when it is near or less than L or δ. The effect of these ratios for the case where the cavity responds as a Helmholtz resonator is not found explicitly in the literature, so it is unclear what the effect is on the current geometry. In any event, the same value of Strouhal number was observed for both depths when $L = 122$ mm, therefore, the effect of depth on the cavity response (apart from its effect on the cavity volume and hence its Helmholtz resonance frequency) is assumed to be negligible.

3. Results and discussion

3.1. Single obstruction

3.1.1. Cavity pressure results

The first comparison of interest is that between an unobstructed opening and the opening with a single obstruction. Spectra at the maximum resonant speed of 33 m/s are shown in Fig. 6 for configurations L0 and L1a. Levels shown in

Table 2
List and description of cavity opening configurations measured

Configuration label	L (mm)	Number of obstructions	Length of obstructions (mm)	Depth of obstructions (mm)	Cavity depth (mm)
S0	122	0	NA	NA	190
S0a	122	0	NA	NA	690
S1	89	1	5	6	190
S13	89	3	5	6	190
S2	89	1	10	6	190
S3	89	1	13	6	190
S4	89	1	19	6	190
S5	89	1	25	6	190
S6	89	1	38	6	190
L1a	289	1	14	22	690
L1b	289	1	25	22	690
L3a	289	3	14	22	690
L0	289	0	NA	NA	690
L1	289	1	3	22	690
L2	289	2	3	22	690
L3	289	3	3	22	690
L5	289	5	3	22	690
L7	289	7	3	22	690
L11	289	11	3	22	690
L23	289	23	3	22	690
I3	289	3	3	22	690
I7	289	7	3	22	690
I3s	289	9	3	22	690
I2s	289	16	3	22	690

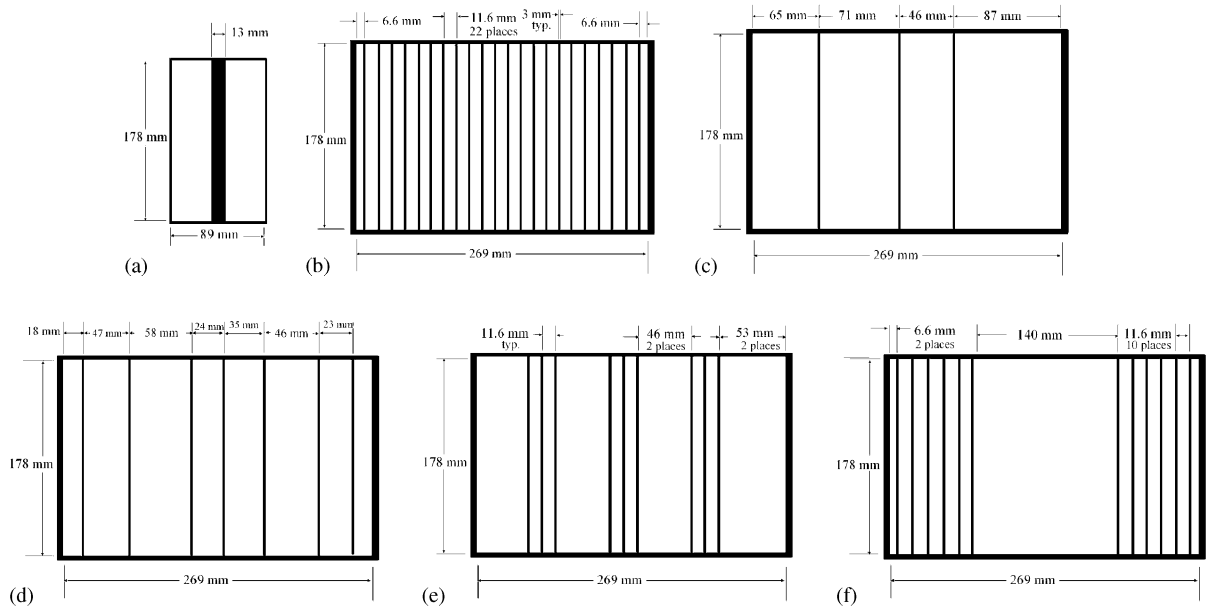

Fig. 5. Drawings showing locations of obstructions in cavity opening for representative configurations. (a) configuration S3; (b) configuration L23; (c) configuration I3; (d) configuration I7; (e) configuration I3s; (f) configuration I2s.

this figure and all subsequent figures are at 1 Hz bandwidth. The effect of the obstruction on the amplitude of the tone is less than 3 dB. The frequency of the tone at the obstructed condition is 2 Hz greater than for the unobstructed case. The reduced area of the opening due to the obstruction will tend to decrease the resonant frequency of the cavity

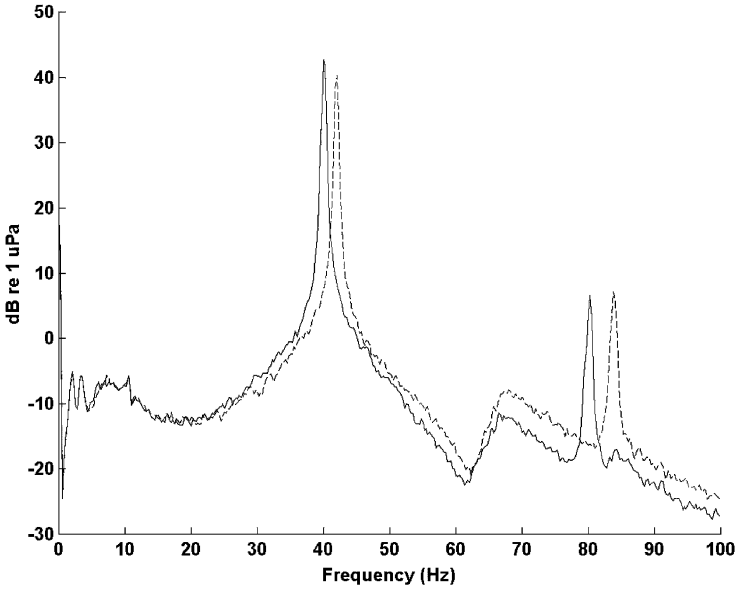

Fig. 6. Cavity pressure spectral density at 33 m/s: ——, configuration L0; - - - - -, configuration L1a.

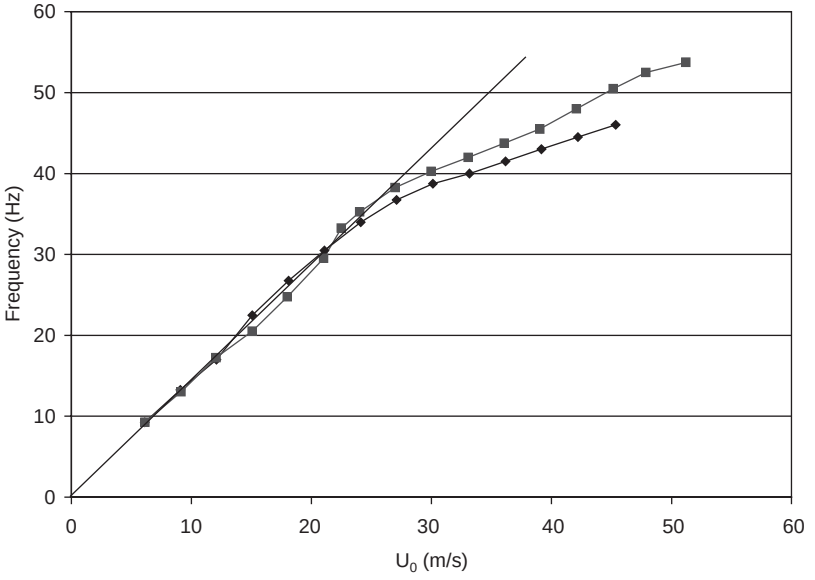

Fig. 7. Frequency of first sheartone observed in the cavity pressure spectra as a function of free-stream velocity: —◆—, configuration L0; —▨—, configuration L1a.

(Kinsler et al. 1982), so that does not explain the frequency difference. The effect of obstruction on frequency is discussed in more detail below in the section on regularly spaced grids.

In Fig. 7 is shown the sheartone frequency as a function of speed for the two configurations compared above. It can be seen that for both configurations at low speeds, the slope is essentially constant. This slope is proportional to the Strouhal number of the sheartone under the nonresonant condition. At approximately 25 m/s, the sheartone becomes coupled to the Helmholtz resonance of the cavity, causing the frequency to increase at a lower rate. The obstruction has no significant effect on the Strouhal number of the sheartone at non-resonant speeds. When the

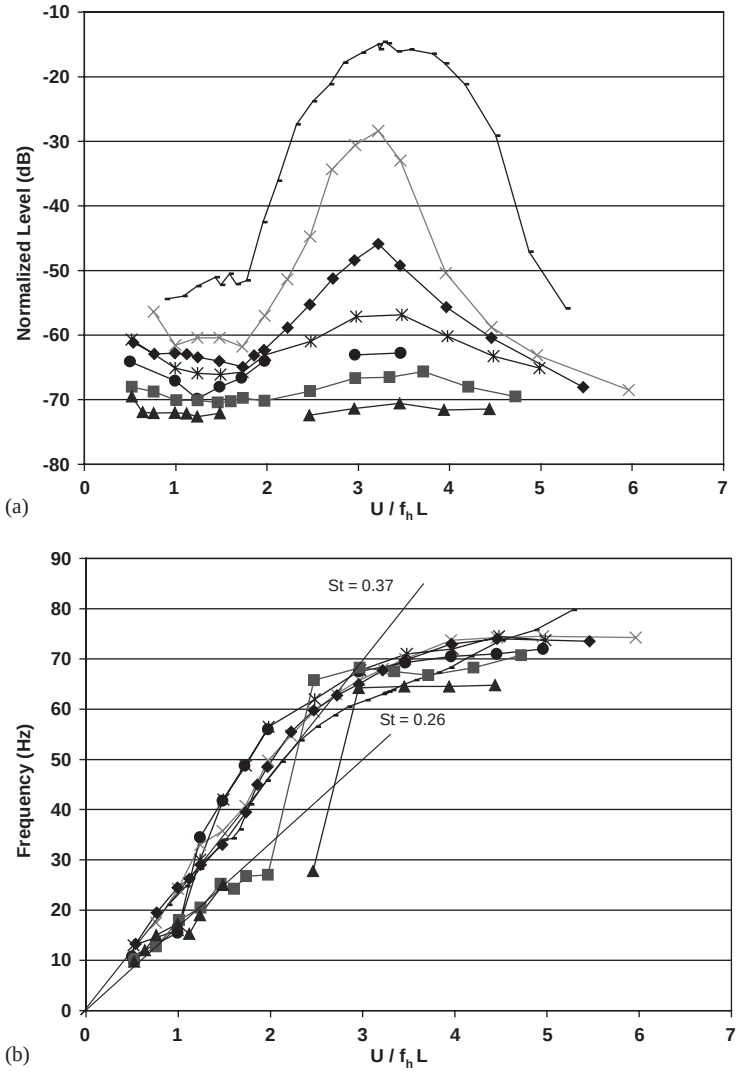

Fig. 8. Frequency and amplitude of first sheartone observed in the cavity pressure spectra as a function of nondimensional velocity U/f_hL for configurations with one obstruction of gradually increasing length in the flow direction. Plot (a) is cavity pressure amplitude normalized by the dynamic head, q. Plot (b) is frequency. —■—, configuration S0; — × —, configuration S1; —◆—, configuration S2; —∗—, configuration S3; —●—configuration S4; —■—, configuration S5; —▲—, configuration S6.

sheartone becomes resonant, it is seen, as it was seen in the spectra above, that the obstruction results in a slight increase in frequency.

The spectra show that a single small obstruction in an opening does not prevent flow-induced cavity resonance at the length scale of the entire opening, but that it does have a slight effect on the amplitude and frequency of the tone. The effect of increasing the size of the obstruction is considered next.

(a) *Effect of obstruction width*. In Fig. 8(a) the amplitude, normalized by the dynamic head, $q = \frac{1}{2}\rho U_0^2$, of the sheartones corresponding to the overall opening length for varying obstruction widths, l, are plotted. These data are for configurations S0, S1, S2, S3, S4, S5, and S6. A drawing of configuration S3 is found in Fig. 5(a). The other configurations were similar, but with different obstructions widths. These are listed in Table 2. The normalized amplitude is shown as a function of the nondimensional velocity, $v^*=U_0/f_hL$, where f_h is the Helmholtz resonance frequency of the cavity. Normalizing the velocity in this way allows comparisons between conditions with different Helmholtz resonance frequencies and opening lengths. It is seen that increasing the width of the obstruction from 5 to

10 mm reduces the maximum amplitude by about 18 dB. Beyond this, each incremental increase in obstruction width decreases the amplitude by a progressively smaller amount. By the time width has been increased to 38 mm, it is not clear from the amplitude results that the observed "tone" may be considered a cavity resonance since the increase in amplitude between resonant and nonresonant speeds is only about 2 dB. That the tone is coupled to the cavity resonance is clearer when the frequencies of the tones are plotted in Fig. 8(b).

In that figure, the frequency behaviors as a function of speed for the 5 and 10 mm obstructions are nearly identical, increasing linearly at lower speeds, where the sheartone is not resonant, and flattening out at higher speeds where the tone is coupled to the cavity resonance. The 13 and 19 mm obstructions also behave similar to each other. However, it is different than the behavior observed for the smaller obstructions. At the lowest speeds the frequency increases at a lower rate than for the smaller obstructions but then the slope increases before beginning to flatten out and falling along the curve traced by the 5 mm obstruction. Finally, the 25 and 38 mm obstructions exhibit the lower slope up until a higher speed before increasing rapidly and then levelling off at frequencies lower than observed with the smaller obstructions.

The decreased slope that results from the larger obstructions translates to a lower value of the Strouhal number of the first sheartone. And unlike in the amplitude results, the reduction is not gradual. The Strouhal number at low speeds for the 5 and 10 mm obstructions, as well as that for the unobstructed opening, are about 0.36, while St for the wider obstructions is about 0.26. From the results of Rossiter (1964), it is known that, at low Mach number, a lower Strouhal number implies a lower value of the convection velocity, U_c, of the vortex along the opening. This suggests that smaller obstructions of, say, $l/L < \sim 0.1$, do not affect the effective convection velocity of the vortex in the opening, while obstructions larger than that reduce the convection velocity by a constant amount.

(b) *Effect of opening length*. The measurements with the 89 mm opening were compared to cavity pressure data for a 269 mm long opening in order to examine how the value of L influences the effect of obstructions in the opening. In Fig. 9, normalized amplitude results for configurations L0, L1a, and L3a, where L is 269 mm, are compared to results for configurations S0, S1, and S13, where L is 122, 89, and 89 mm, respectively. No unobstructed 89 mm data were available. It may be seen that while the length of the opening has a small effect on the amplitude for an unobstructed opening, it has an increasing effect for increasing numbers of obstructions. This effect is more pronounced for the smaller value of L. A single obstruction reduces the amplitude by about 3 dB in the longer opening but by nearly 20 dB in the shorter opening. And for three obstructions, in an unobstructed opening they reduce the maximum amplitude by about 20 dB in the long opening, but by over 40 dB in the short opening. It should be noted that the observed difference in the value of v^* at which the maximum amplitude occurs is likely due to the effect the different values of δ/L have on the frequency of the sheartone excitation. The effect of boundary layer properties on frequency was examined in detail by Zoccola and Farabee (2001), who found that the frequency of a nonresonant sheartone is proportional to $(\theta/L)^{-1/6}$,

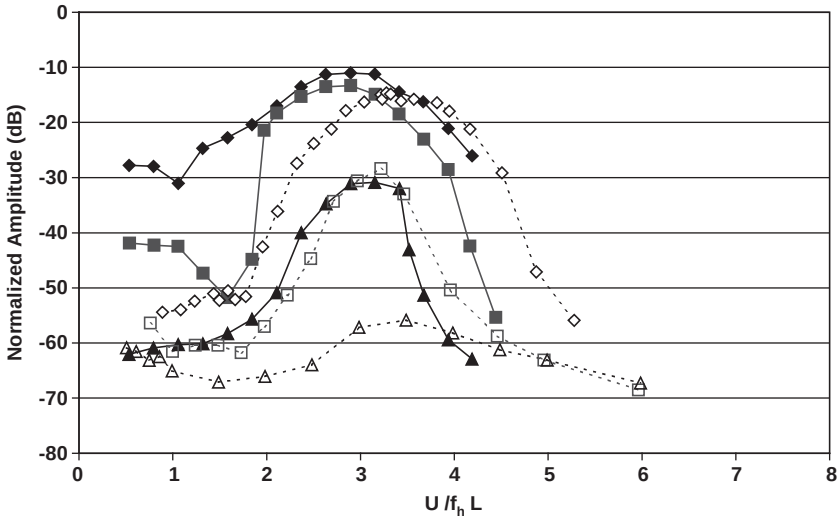

Fig. 9. Comparison of cavity pressure amplitude normalized by the dynamic head, q, for two different values of cavity opening length, L. Solid lines represent data for $L = 269$ mm; dotted lines represent data for $L = 89$ mm. Symbols represent varying numbers of obstructions in the opening: —◆—, configuration L0; —▨—, configuration L1a; —▲—, configuration L3a; - - -◇- - -, configuration S0; - - -□- - -, configuration S1; - - -△- - -, configuration S13.

where θ is the momentum thickness of the onset boundary layer. It is likely that a significant change in the boundary layer would also affect the amplitude due to flow over an obstructed opening. However, data for different boundary layer properties were not available.

3.1.2. Mean flow

In the first phase of the experiment, flow field measurements were made for configuration L1a at 17 m/s, where the resonance is excited to its maximum amplitude at the 122 mm length scale created by the obstruction, and at 30 m/s, where the resonance is excited to its maximum amplitude on the 269 mm length scale. During flow measurements in this phase of the experiment, the probe was positioned at locations making up a grid of 10 locations in the y direction by 41 locations in the x direction. The y locations ranged from -36 to 36 mm, centered at $y=0$ and spaced more closely near the center; some y locations were altered near the obstruction in the opening. The x locations were spaced 6 mm apart. Flow field measurements were also made for configuration S0a at the maximum resonance speed of 14 m/s. In Fig. 10, the mean velocity vectors for configuration L1b at 17 and 30 m/s are shown. A comparison reveals that the mean flow field is very similar for these two conditions. The only, minor, difference worth noting is that at the downstream edge for 30 m/s, the vectors near the flow surface appear to have a larger v component than is observed at the downstream edge for 17 m/s. It is unclear whether this difference is related to the different nature of the tone at these two speeds.

3.1.3. Phase

The phase between v, the fluctuating flow in the wall normal direction, and the cavity pressure at the frequency of excitation is also considered. This quantity is shown in Fig. 11 for configuration L1b at 17 and 30 m/s. Nelson et al.

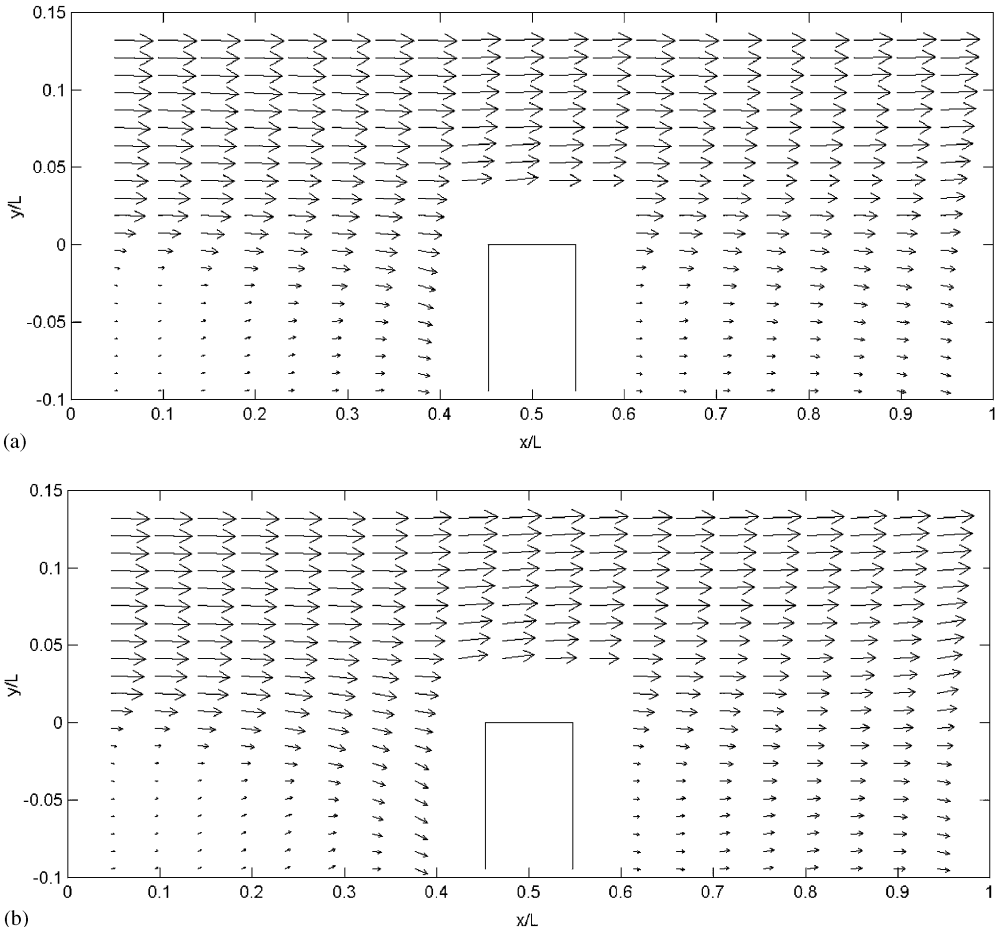

Fig. 10. Plot of vectors representing mean flow velocity in the opening for configuration L1b at (a) $U_0=17$ m/s and (b) $U_0=30$ m/s.

(1983) showed that for a conventional cavity opening at resonance, this phase goes through about 1 cycle between the upstream and downstream edges of the opening. Ziada and Rockwell (1982) also note that for a mixing layer impinging on an edge, the phase of the velocity fluctuations between the upstream and downstream edges is $2n\pi$, where n is an integer. For the 17 m/s condition, where the resonance occurs at the 122 mm length scale created by the obstruction, the phase does move through about 1 cycle in the 122 mm both upstream and downstream of the obstruction. This suggests that each half of the opening acts as a single122 mm opening would. It should be noted that the actual value of the phase (mod 360) is somewhat different between the upstream and downstream openings, however that need not prevent both openings from exciting the cavity.

At 30 m/s, the phase increases by about 1 cycle over the full 269 mm length of the obstructed opening. This is consistent with a Strouhal number based on $L = 269$ mm having a value similar to that observed in the cavity pressure results. The phase results suggest that the obstruction does little to impede the vortex. Some small regions of anomalous phase are present just downstream of the obstruction, but these do not appear to impact the overall phase behavior.

3.1.4. Energy production

How the flow drives the cavity may be considered by studying the distribution of the mean energy production in the opening. The energy production term, which was derived by Nelson, et al. (1983), considers the interaction between the fluctuating vorticity, mean flow, and acoustic particle velocity. This interaction results in an acoustic energy balance in which acoustic energy flows into the cavity near the downstream edge. Some of this energy is absorbed by interactions in the upstream half of the opening. The remaining energy is dissipated by some combination of acoustic radiation and energy carried away by the vortices.

To derive the energy production term, Nelson starts with the energy transport equation developed by Doak (1974) and derives the following expression for the net power, W_v, extracted from the mean flow:

$$W_v = \int_v [-(\rho \mathbf{u})' \cdot (\Omega \times \mathbf{u})'] \mathrm{d}V,$$

where Ω is the vorticity vector, $\mathbf{u}$ is the velocity vector, ρ is the fluid density, and the integration is performed over the region of nonvanishing vorticity, V. The prime denotes the fluctuating component of the quantity and the overbar refers denotes the time average.

For two-dimensional flow in the opening, the integral may be reduced to

$$W_v = \int_v [-\rho_0 \bar{u}\, \overline{\Omega_3' v'}] \mathrm{d}V,$$

where Ω_3' is the fluctuating part of the vorticity in the z direction, v' is the fluctuating part of the flow in the y direction and u is the flow in the x direction. The energy production term is the quantity in the integral. It represents the interaction between the fluctuating Coriolis force and the fluctuating velocity and is a measure of the energy transferred from the mean flow to the fluctuating flow. For this experiment, the energy production term was estimated by averaging the instantaneous product of Ω_3' and v' and multiplying by u. This was done at each measurement location. The vorticity, Ω_3', was estimated by taking the approximating the differentials in the equation for vorticity by the differences between points in the x and y directions. Because the results are discussed only in a qualitative sense, the effect of descretization errors was not considered.

In their paper, Nelson et al. show calculations of energy production for a flow-excited cavity opening. The results show a region of positive energy production (source) near the downstream edge and a region of negative energy production (sink) in the upstream half of the opening. Reasonably good agreement with this result was found by Zoccola (2000), who reported measurements of the energy production term distribution for conventional cavity opening which showed regions of positive and negative energy production in the opening, with the positive being of greater magnitude and positioned above and somewhat downstream from the negative region. Essentially the same distribution was observed for measurements on configuration S0a at 14 m/s.

Distributions of the energy production term for configuration L1b at 17 and 30 m/s are shown in Fig. 12. The distributions for the upstream and downstream halves of the opening at 17 m/s are similar to that for the unobstructed opening at 30 m/s, though in the downstream half, the negative region is weaker, smaller and further upstream. At 30 m/s, where the full 269 mm is the length scale of the excitation, the expectation was that a pattern like that for the unobstructed opening would be seen, but would be spread across the full span of the opening. Instead, in the upstream part of the opening, the pattern was similar to that seen at 17 m/s, though the positive region is seen to extend past the upstream part of the obstruction, and the negative region is further downstream. In the downstream part of the opening, the positive region has a significantly lower magnitude. A visual comparison between the 17 and 30 m/s conditions suggests that while the disruption of the phase along the opening due to the convection of the vortex is

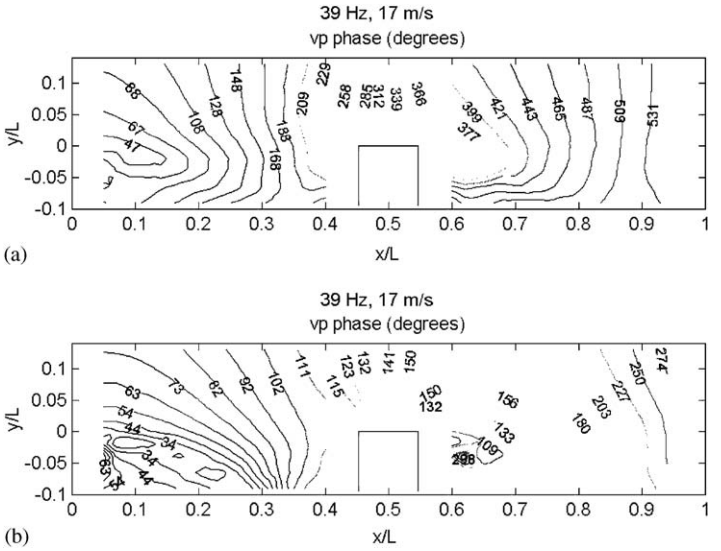

Fig. 11. Contour plot showing phase in the cavity opening with configuration L1b at 39 Hz between flow velocity in y (out-of-plane) direction, v, and cavity pressure, p, at (a) $U_0 = 17$ m/s and (b) $U_0 = 30$ m/s.

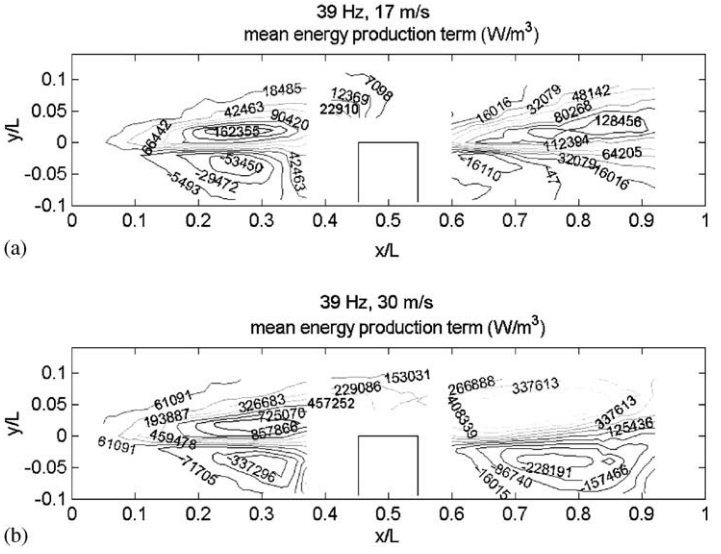

Fig. 12. Contour plot showing value of energy production term at 39 Hz in the cavity opening with configuration L1b at (a) $U_0 = 17$ m/s and (b) $U_0 = 30$ m/s.

relatively unaffected by the presence of the obstruction, its effect on the energy production is more significant. The values of the velocity and vorticity and the relationship between them are disrupted in such a way that energy production does not occur in the region near the obstruction. In the region beyond the obstruction, these quantities do not have sufficient space or time to achieve the state they were in upstream of the obstruction.

3.1.5. Convection velocity

The influence of an obstruction on the mean convection velocity of the vortex in the opening was discussed in Section 3.1.1. It is also useful to consider the behavior of the local convection velocity. The local convection velocity of the

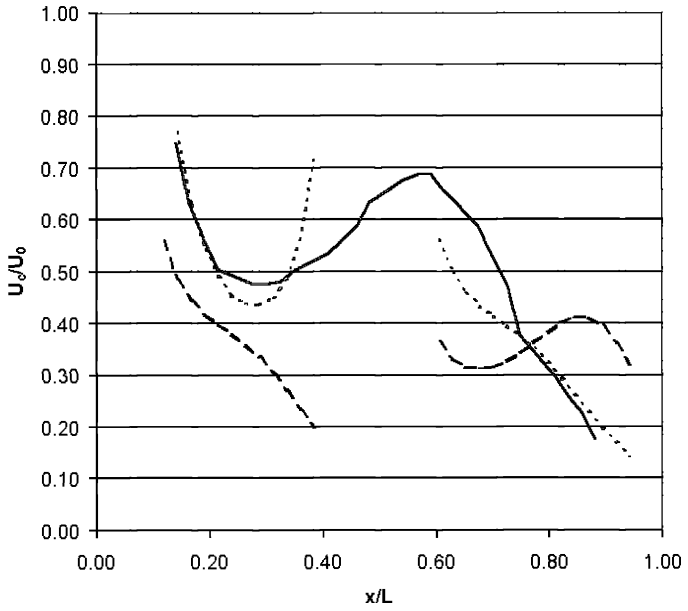

Fig. 13. Plot of local convection velocity of vortex in the cavity opening for configuration L0 at 30 m/s (——), L1b at 17 m/s (– – –), and L1b at 30 m/s (▪▪▪▪▪▪▪▪▪).

vortex is essentially the phase speed of the disturbance as it moves along the opening. This quantity can be calculated from the phase between the cavity pressure and the velocity fluctuations in the out of plane direction. The derivative along the streamwise dimension, x, of the phase, ϕ, between the out of plane velocity and the cavity pressure, $\mathrm{d}\phi/\mathrm{d}x$, is effectively the wavenumber, k, of the disturbance. Wavenumber is related to frequency by $k = \omega/U_c$, where U_c is the phase speed, or convection velocity and ω is the angular velocity, $2\pi f$. The derivative can be taken and the result rearranged to give $U_c = 2\pi f/(\mathrm{d}\phi/\mathrm{d}x)$. For the data shown, the derivatives were taken at the y location corresponding to the maximum vorticity in the y direction.

Plots of convection velocity as a function of streamwise distance, x, for configuration L1b at 17 and 30 m/s, and for configuration L0 at 30 m/s, are shown in Fig. 13. The convection velocity is normalized by the free-stream velocity, and x is normalized by the overall length of the opening. The unobstructed condition is essentially a baseline, and is similar to the results reported in Zoccola (2000), who showed that for flow over an unaltered opening, the vortex decelerates as it approaches the downstream edge. For the 17 m/s condition, the convection velocity in the upstream half of the opening shows essentially the same behavior as the baseline condition. This is consistent with results discussed above, where the phase and energy production in the upstream half of the opening for the 17 m/s condition showed behavior essentially the same as the baseline condition.

The downstream half of the opening at 17 m/s behaves differently. But it remains the case that here, as in the upstream half and the baseline condition, and indeed, for all conditions reported in Zoccola (2000), the vortex decelerates as it approaches the downstream edge, or, in the case of the 17 m/s condition, the obstruction. However, for the 30 m/s condition, the convection velocity, like the energy distribution, the behavior of U_c over the 269 mm length scale is not the same as the scaled baseline condition. In the upstream half of the opening, it can be seen that the vortex accelerates as it approaches the obstruction.

3.2. Gridded opening

3.2.1. Cavity pressure results

(a) *Regularly spaced grid.* In the second phase of the experiment, measurements of cavity pressure fluctuations were made on openings with grids composed of various numbers of obstruction. The obstructions were equally spaced, with the exception of minor variations at the upstream and downstream edges. Configurations measured were L0, L1, L2, L3, L5, L7, L11, and L23. Configuration L23 is shown in Fig. 5(b); the other configurations were created by removing grid elements from the locations shown in that figure. Data were collected in approximately 3 m/s increments at speeds

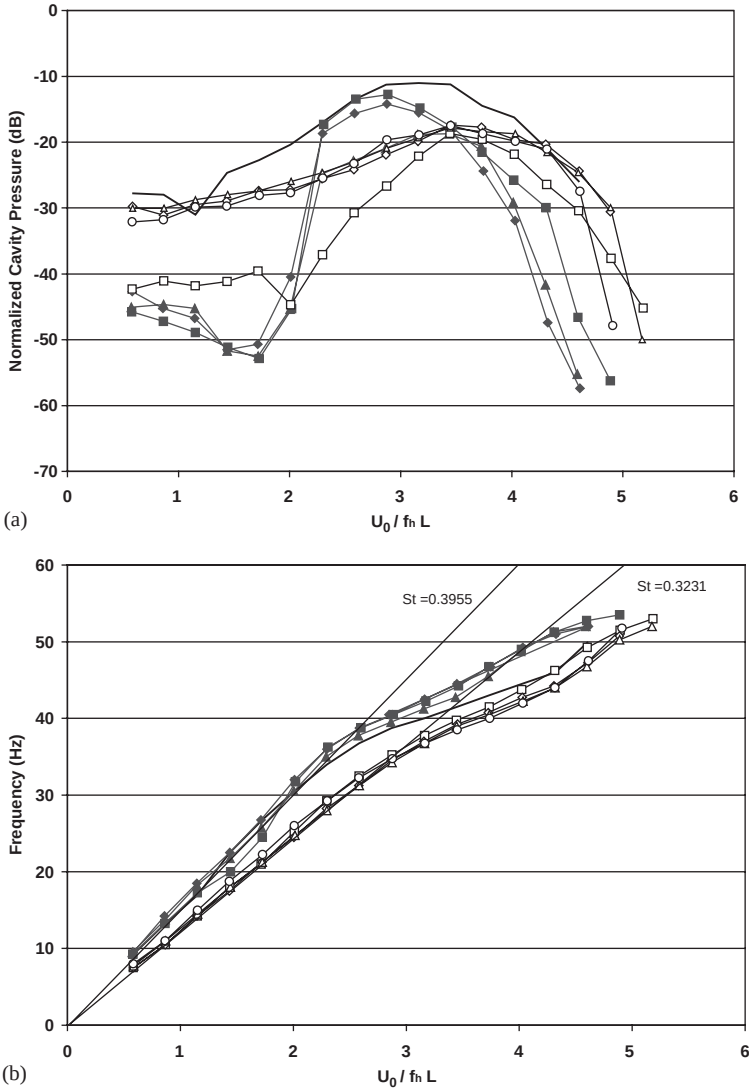

Fig. 14. Frequency and amplitude of first sheartone observed in the cavity pressure spectra as a function of nondimensional velocity U/f_hL for configurations with varying numbers of grid elements. Plot (a) is cavity pressure amplitude normalized by the dynamic head, q. Plot (b) is frequency: ——, configuration L0; —■—, configuration L1; —◆—, configuration L2; —▲—, configuration L3; —□—, configuration L5; —◇—, configuration L7; —△—, configuration L11; —○—, configuration L23.

between 6 and 54 m/s. The amplitude of the measured first sheartone as a function of speed is shown for each configuration in Fig. 14(a). In Fig. 14(b), the frequency versus speed of that same sheartone is shown.

What is most significant about these data is the distinct difference between the results for a coarse grid (three or fewer obstructions) and those for a fine grid (five or more obstructions). At low speeds, where the sheartone is not coupled with the Helmholtz resonance of the cavity, the fine grids show amplitudes similar to that for an undivided opening, and much greater than the amplitudes seen with a coarse grid. At higher speeds, however, data with a coarse grid have higher amplitudes, the maximum being nearly equal to that for an undivided opening. Configuration L5 demonstrates a transition between the two behaviors of the amplitude data.

The frequency results show the same distinct difference between the behavior with a coarse and a fine grid. The slopes of the frequency curve in the low-speed range are essentially the same for the undivided opening and for all openings with a coarse grid. The slope with a fine grid present is lower. As indicated on the figure, the coarse grid has a St of 0.40, while the fine grid has St = 0.32.

A possible explanation for the difference in frequency behavior with coarse and fine grids is likely the same as for the frequency behavior seen with different obstruction widths: a fine grid reduces the convection velocity of the vortex in the opening. And like the obstruction width results, there is no gradual reduction in Strouhal number; for coarse grids it has one value, and for fine grids a lower one. However, unlike the obstruction width results, the amplitude behavior for fine and coarse grids also shows a distinct difference between the two, with only one configuration appearing to transition between the behavior observed for coarse and fine grids.

(b) *Irregularly spaced grid*. In all of the configurations discussed above, the elements of the grid were approximately equally spaced. The possibility had been suggested that the results obtained may have been related to the regular spacing of the obstructions. Therefore, additional data were taken in order to understand the effect that irregular spacing of grid elements would have on the results.

In Fig. 15, data are shown for configurations I3 and I7. Also shown for comparison purposes are the comparable regularly spaced grid results from configurations L3 and L7. The distribution of the elements for the irregularly spaced configurations was chosen so as to ensure that the spacing between elements was obviously not constant nor according

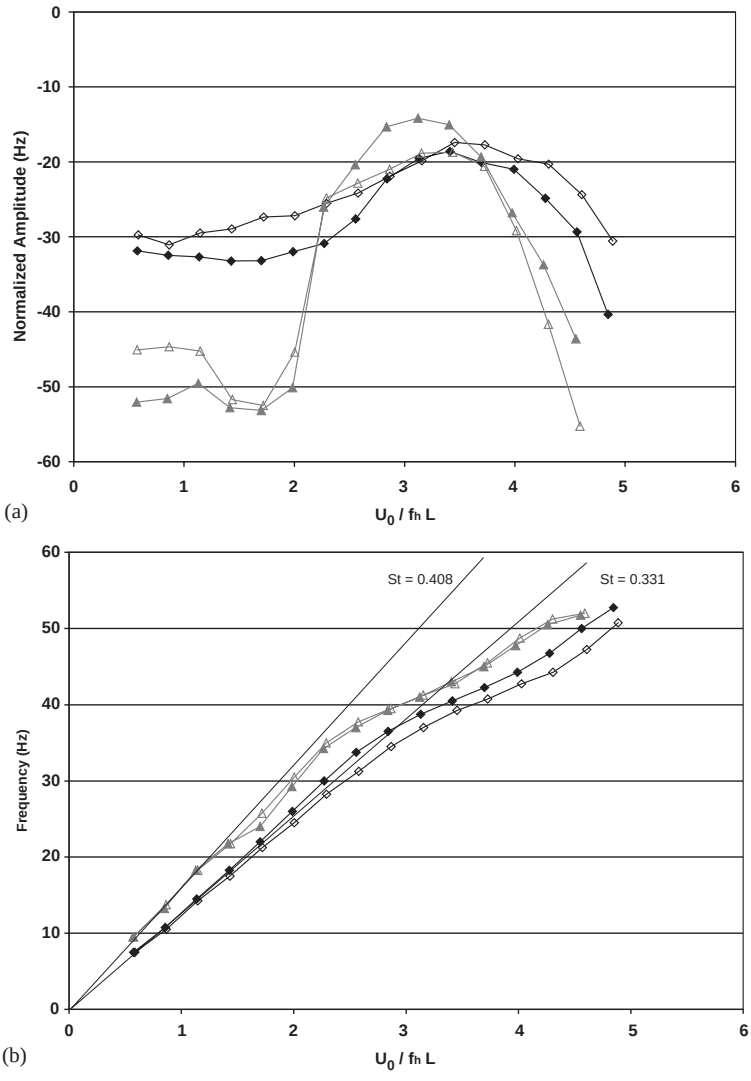

Fig. 15. Frequency and amplitude of first sheartone observed in the cavity pressure spectra as a function of nondimensional velocity U/f_hL for two different configuration with irregular spacing of grid elements. Comparison is made with the same number of elements regularly spaced. Plot (a) is cavity pressure amplitude normalized by the dynamic head, q. Plot (b) is frequency: —▲—, configuration I3; —△—, configuration L3; —◆—, configuration I7; —◇—, configuration L7.

to any kind of repeatable pattern, while also taking care not to allow any element to be so close to any other so as to act as a larger element cluster. The results show essentially the same behavior that was seen for regularly spaced grids, with I3 behaving like a regularly spaced coarse grid, and I7 behaving like a regularly spiced fine grid.

In addition to the irregularly spaced configurations described above, several configurations were measured to determine the effect of having clusters of closely spaced grid elements. The first, configuration I3 s is similar to the configuration L3, except that rather than 1 grid element at each of three locations, 3 closely spaced elements are placed at each location. The second, configuration I2 s, has the opening divided approximately into thirds. The front third and the back third are filled with elements spaced as were those for the opening divided into 24ths; the middle third is open.

The results for these configurations are shown in Fig. 16. Also shown for comparison are configurations I3, L2, and L7. In the frequency results, it is seen that configuration I2 s behaves substantially like configuration L2, which represents the regularly spaced coarse grid conditions. That is, despite the forward and aft third being fine grids, the open middle third results in the condition behaving as if it were an opening divided into thirds. Configuration I3 s, however, did not behave like a coarse grid. Its frequency behavior is more or less half way between that of a coarse and a fine grid, represented by configuration L7.

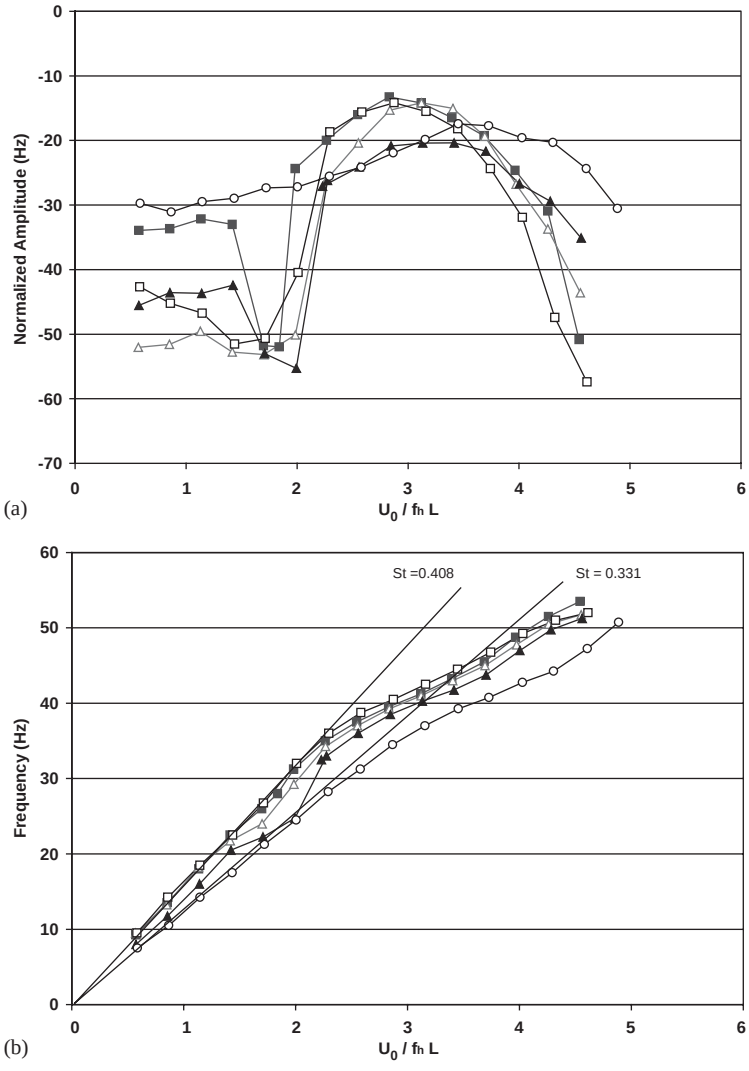

Fig. 16. Frequency and amplitude of first sheartone observed in the cavity pressure spectra as a function of nondimensional velocity U/f_hL for two different configuration with irregular spacing of grid elements. Comparison is made with the other regularly and irregularly spaced conditions. Plot (a) is cavity pressure amplitude normalized by the dynamic head, q. Plot (b) is frequency: —■—, configuration I2s; —▲—, configuration I3s; —△—, configuration I3; —□—, configuration L2; —○—, configuration L7.

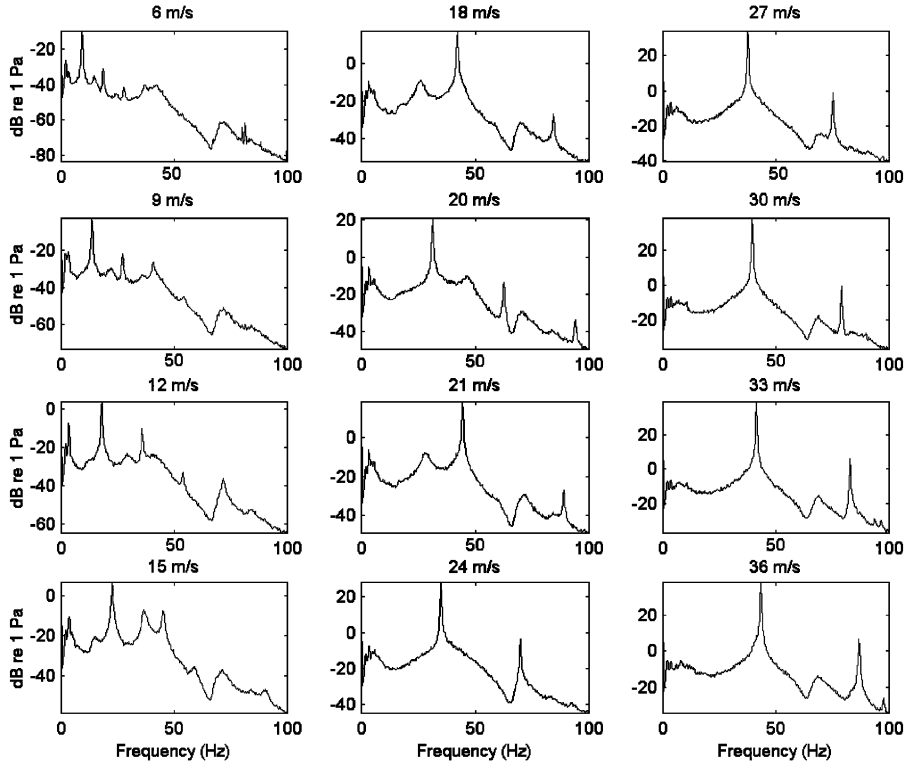

Fig. 17. Cavity pressure spectral density at 12 speeds for condition I2s.

The amplitude behavior of these conditions is similar to the frequency behavior, but with an important exception. In the high speed range, I2 s follows the coarse grid behavior and I3 s seems to be about half way between coarse and fine. However, their behavior in the low speed region is unlike either fine or coarse. I2 s has amplitudes typical of fine grids at the low speed end but then drops down to coarse grid amplitudes before the increase in amplitude associated with lock in to the cavity resonance. I3 s has amplitudes half way between fine and coarse at the low end but then also drops down to coarse amplitudes prior to locking in.

An explanation for this may be found by considering the effect that these conditions have on the second sheartone. Fig. 17 shows the spectra at 12 speeds for configuration I2 s. At 18 and 20 m/s, the amplitude of the first sheartone, at about 27 Hz is substantially less than at the other speeds. But the amplitude of the second sheartone is much greater than at the other speeds. The spectra of the evenly spaced coarse grids show that the amplitude of the second sheartone is higher than that of the first at all of the speeds prior to locking in to the cavity resonance, while the spectra of the evenly spaced fine grids show weak or nonexistent second sheartones at all speeds. It seems that the amplitudes of the first sheartones at low speed depend on the effect that the grid has on the second sheartone. Fine grids weaken the second sheartone, allowing the first sheartone to have a higher amplitude at lower speeds. Coarse grids affect the second sheartone to a much lesser degree, so the energy extracted from the mean flow by the second sheartone is the reason for the low amplitudes in the low speed region of coarse grid configuration. The irregularly spaced grids considered here have varied effects on the second sheartone, and that effect is reflected in the low-speed amplitude behavior.

3.2.2. *Energy production*

For flow field measurements made during the this phase of the experiment, the probe was positioned at 311 locations within the opening. These locations made up a grid of 11 locations in the y direction by 29 locations in the x direction. The y locations ranged from -36 to 36 mm, centered at $y=0$ and spaced more closely near the center. The x locations were spaced at approximately 6 mm apart, with the spacing altered as needed to avoid interfering with grid elements in the opening. Fig. 18 shows contour plots of the energy production term distribution at 9 m/s for the unobstructed, coarse grid and fine grid configurations L0, L3, and L8, respectively. At this speed, the sheartone is not coupled to the cavity resonance. The L8 and L0 both show significant regions of negative energy production, though the magnitude of that region for the fine grid is lower. Configuration L3 shows essentially no region of negative energy. This more or less

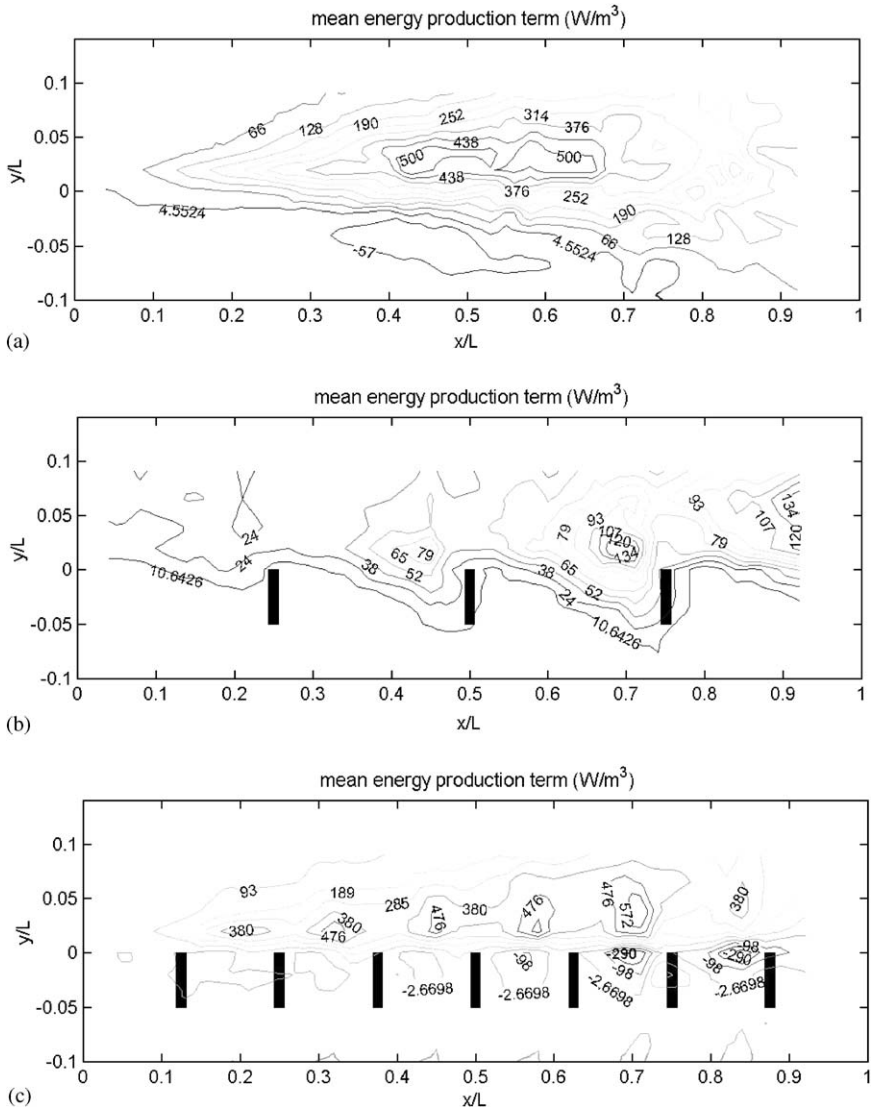

Fig. 18. Contour plot showing value of energy production term at frequency corresponding to the first sheartone in the cavity opening with $U_0 = 9$ m/s for three configurations. (a) configuration L0; (b) configuration L3; (c) configuration L7.

conforms with the discussion with the previous section, where it was seen that there is a lower amplitude of the first sheartone for the coarse grid and that this is likely due to the strong presence of the second sheartone here, while it is suppressed by the fine grid.

In Fig. 19, contour plots of the energy production term distribution for the same configurations in the resonant condition at 30 m/s are shown. Fig. 19(a) shows for the unobstructed case the regions of positive and negative energy productions seen in the data from Zoccola (2000) and predicted by Nelson et al. (1983). The coarse and fine grids appear to have the effect of "smearing" these regions in the streamwise direction. The results for both grids could also be interpreted as having a positive and negative region associated with each space between obstructions. These results seem consistent with the results for condition L1a discussed above, where the region downstream of the obstruction could be interpreted both as a single region pair of positive and negative regions disturbed by the obstruction or as two-independent pairs, the downstream being rather weaker.

It is also worth noting that the distribution for the fine grid is substantially the same at both low and high speeds, which is not the case for the other two conditions. This is likely due to the fact that, due to experimental limitations, the high speed data is somewhat below the maximum resonant speed.

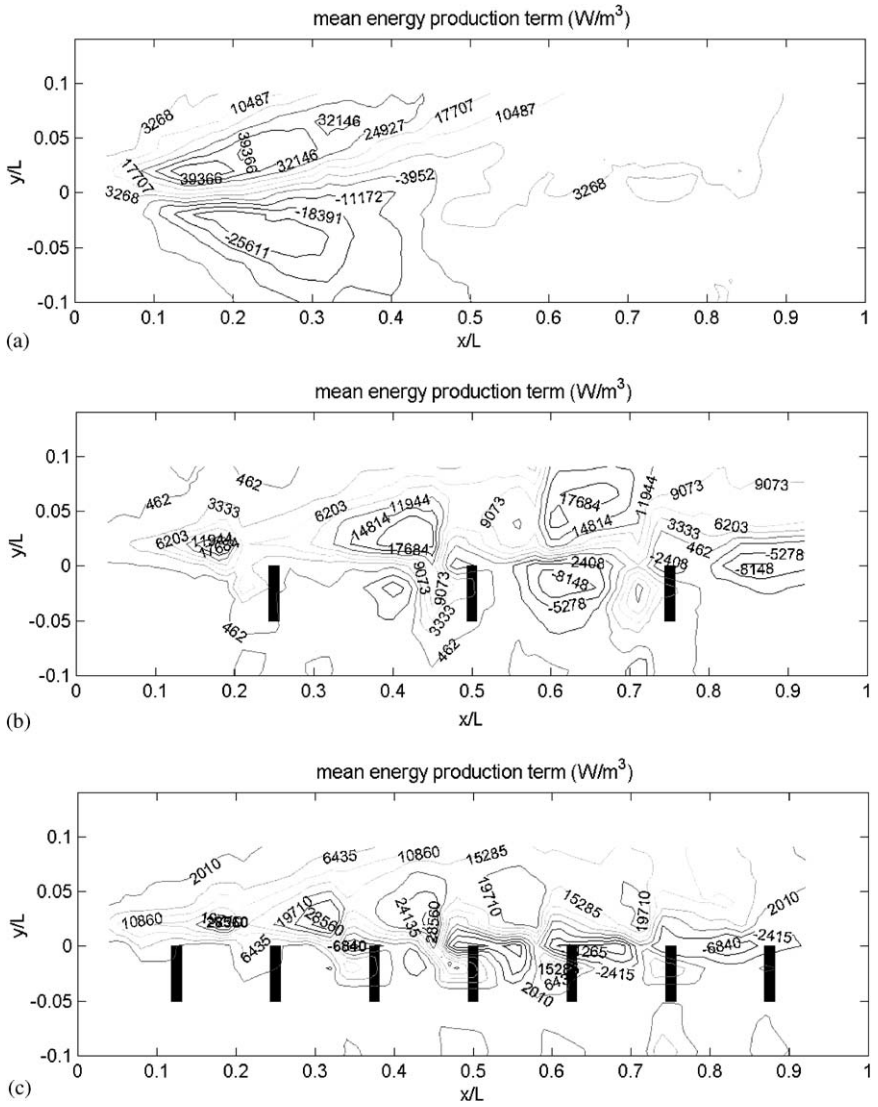

Fig. 19. Contour plot showing value of energy production term at frequency corresponding to the first sheartone in the cavity opening with $U_0 = 30$ m/s for three configurations. (a) configuration L0; (b) configuration L3; (c) configuration L7.

4. Conclusions

It has been confirmed experimentally that flow over an opening can excite a cavity to resonate at frequencies scaling on the full length of the cavity opening when an obstruction or grid of regularly spaced obstructions are present in the opening. While excitation at the large length scale occurs with an obstructed opening, the obstructions still have an effect on the amplitude of the measured cavity pressure. Results of measurements over a broad range of flow speeds with a single obstruction show that increasing the width of the obstruction element reduces both the amplitude and the frequency of the response. The magnitude of the amplitude reduction appears to depend on the streamwise length of the opening for a given inflow boundary layer.

The results of cavity pressure measurements with various grids revealed a distinct difference in the amplitude versus speed and frequency versus speed behavior with fine versus coarse grids. A coarse grid is one composed of three or fewer obstructions, and a fine grid is one composed of four or more obstructions. There was no gradual transition between the two behaviors observed. A coarse grid had no effect on the Strouhal number of the tone, while all fine grids had the same, lower, Strouhal number. Also, the fine grid seemed to have the effect of eliminating

the second-order tone, resulting in higher amplitudes of the first-order tone at low speeds compared to the coarse grid. At higher speeds, the coarse grid had only a small effect on the amplitude while the fine grid had a greater effect.

Results with various irregularly spaced grid elements showed that regular spacing of the grid elements was not necessary to the effects observed. They also showed that clusters of closely spaced elements could sometimes act like single elements, as could alternating regions of fine grid and no grid elements.

Measurements of the flow field in an opening with a single obstruction confirmed the pressure results. They showed that, at resonant excitation corresponding to the smaller length scale created by the obstruction, the flow quantities of phase and energy production showed distributions over the smaller length scale similar to what would be found for an unobstructed opening. For large length-scale excitation, those quantities are distributed in a similar pattern across the overall length, with some minor effects due to the presence of the obstruction observed.

The obstruction had a more significant effect on the local convection velocity of the vortex in the opening. When excitation occurs at the length scale created by the obstruction, the obstruction behaves like a typical downstream edge, causing the vortex to decelerate, whereas at the larger length scale, the vortex appears to accelerate past the obstruction.

Measurements of the flow field with coarse and fine grids generally yielded results that were consistent with the results of the pressure field measurements. The distribution of the energy production term for the various speeds and grids showed regions of positive and negative energy at speeds where the pressure amplitude was highest. The grid elements appear to create individual regions of energy production at each element, resulting in a large, smeared, energy production region when compared to an unobstructed opening.

Acknowledgements

The sponsorship of this work by the In-house Laboratory Independent Research (ILIR) Program at NSWC Carderock Division is gratefully acknowledged. Thanks are also due to Mr Thomas Mathews for his essential assistance in the conduct of the experiment.

References

Celik, E., Rockwell, D., 2002. Shear layer oscillation along a perforated surface: a self-excited large-scale instability. Physics of Fluids 14, 4444–4447.

DeMetz, F.C., Farabee, T.M., 1977. Laminar and turbulent shear flow-induced cavity resonances. AIAA Paper No. 77-1293.

Doak, P.E., 1974. Acoustic, thermal, and turbulent energy density and linear momentum density relationships and flux in fluctuating flows. In: Proceedings of the Eighth International Congress on Acoustics, Contributed Papers, Vol. II, p. 532.

Elder, S.A., 1978. Self-excited depth-mode resonance for a wall-mounted cavity in turbulent flow. Journal of the Acoustical Society of America 64, 877–890.

Farabee, T.M., Casarella, M.J., 1984. Effects of surface irregularity on turbulent boundary layer wall pressure fluctuations. ASME Journal of Vibration, Acoustics, Stress, and Reliability in Design 106, 343–350.

Grega, L., Farabee, T.M., 1997. Experimental investigation of the influence of pressure gradients on floodport noise. NSWCCD-SIG-C97/133-7250.

Howe, M.S., 1997. Edge, cavity and aperture tones at very low mach numbers. Journal of Fluid Mechanics 330, 61–84.

Kinsler, L.E., Frey, A.R., Coppens, A.B., Sanders, J.V., 1982. Fundamentals of Acoustics. Wiley, New York.

Kook, H., Mongeau, L., 2002. Analysis of the periodic pressure fluctuations induced by flow over a cavity. Journal of Sound and Vibration 251, 823–846.

Looijmans, K.N.H., Bruggeman, J.C., 1997. Simple vortex models for vibration and noise caused by a flow over louvers in a cavity opening. In: Paidoussis (Ed.), Fluid–Structure Interaction, Aeroelasticity, Flow-Induced Vibration and Noise, Vol. 1, ASME, NewYork.

Mast, T.D., Pierce, A.D., 1995. Describing-function theory for flow excitation of resonators. Journal of the Acoustical Society of America 97, 163–172.

Nelson, P.A., 1982. Noise generated by flow over perforated surfaces. Journal of Sound and Vibration 83, 11–26.

Nelson, P.A., Halliwell, N.A., Doak, P.E., 1983. Fluid dynamics of a flow excited resonance, part II: flow acoustic interaction. Journal of Sound and Vibration 91, 375–402.

Rockwell, D., Knisely, C., 1979. The organized nature of flow impingement upon a corner. Journal of Fluid Mechanics 93, 413–432.

Rockwell, D., Naudasher, E., 1978. Review—self-sustaining oscillations of flow past cavities. ASME Journal of Fluids Engineering 100, 152–165.

Rossiter, J.E., 1964. Wind tunnel experiments on the flow over rectangular cavities at subsonic and transonic speeds. RAE Technical Report 64037.

Sarohia, V., 1977. Experimental investigation of oscillations in flows over shallow cavities. AIAA Journal 15, 984–991.

Tsui, C.Y., Flandro, G.A., 1977. Self-induced sound generation by flow over perforated duct liners. Journal of Sound and Vibration 50, 315–331.

Ziada, S., Rockwell, D., 1982. Oscillations of an unstable mixing layer impinging upon an edge. Journal of Fluid Mechanics 124, 307–334.

Zoccola, P.J., 2000. Experimental investigation of flow induced cavity resonance. Ph.D. Thesis, The Catholic University of America; also available as NSWCCD Report NSWCCD-TR-2000/010.

Zoccola, P.J., Farabee, T.M., 2001. On the frequency of sheartones. Acoustic Research Letters Online 2, 13–18.